PAPER ID: 11A11U

FIELD MEASUREMENT AND SIMULATION VALIDATION OF INCIDENT IRRADIANCE ON VERTICAL FACADE IN TROPICAL COUNTRIES

Azhar Ghazali [1*], Lim Chin Haw [2]

[1] School of Housing, Building, and Planning, Universiti Sains Malaysia, MALAYSIA.
[2] Solar Energy Research Institute, Universiti Kebangsaan Malaysia, MALAYSIA.

A R T I C L E I N F O	A B S T R A C T
	The comprehension of sun-powered radiation and the position of the sun is very crucial for photovoltaic application to ensure the photovoltaic module operate at an optimum level at any given site and orientation. To facilitate the growth of photovoltaic utilization, forecasting the solar irradiance using simulation tools has become an effective predictive measure to forecast the photovoltaic power generation. However, the accuracy of prediction in the simulation tool needs to verify through the validation process. This experiment was performed in the field test and the calculated data from this measurement was used to verify the data from the simulation. This study examines the errors and precision of the forecast model in the simulation system, based on the recommended validation measures. This field experiment covers eight different vertical façade configurations. The result indicates that vertical façade to the east and west exposed the most incident radiation.

Disciplinary: Architectural Sciences, Renewable Energy

©2020 INT TRANS J ENG MANAG SCI TECH.

1. INTRODUCTION

For photovoltaic (PV) technology applications, the availability of direct solar exposure is essential to evaluate its electrical performance (Madhu and Gangadharan, 2016). In the evaluation process, the level of irradiance should be evaluated to ensure that the operation of the PV system is beneficial (Mohanty et al. 2015).

Solar radiation is classified as radiant energy (electromagnetic energy) emitted by the sun, (Markvart. 2002). Due to normal daily and annual variability caused by the apparent motion of the sun, irregular climate shifts, and cloud cover, the amount of solar radiation reaching the ground is greatly unpredictable.

2. LITERATURE REVIEW

Design and resource optimization in the PV technology project is the two phases require to forecast and assess the power generation. Such measures require specific solar radiation data assessment. The design stage offers the requisite data for the configuration of the PV system and the feasibility studies. In the development stage, the average value of solar irradiation or Typical Meteorological Year (TMY) is adequate (Janjai and Deeyai, 2009). In the exploitation activity, however, demanded more precise solar radiation data estimate the system's power output for the optimal operating period. Projections of solar irradiance are not expected to vary significantly from the estimates of PV power generation (Espinar et al. 2010) as PV electricity production is strongly linear based on global irradiance level (Mayer et al. 2008).

Solar irradiance forecasts help the PV system operators to monitor the electricity supply for both near-term (system reserves and distribution) or longer-term (unit commitment and scheduling) duration (Nobre et al. 2016). The reliability of forecasting energy output at the PV plant gas a significant impact on the system's financial operation and therefore on the price of electricity produced from the plant (Parson et al. 2005; Ortega-Vasquez et al. 2010). Nonetheless, inaccuracies in the prediction of solar irradiance and the PV power production could have major economic implications (Denholm and Margolis, 2007). It is very important to gain a better comprehension of solar activity particularly in tropical region countries where the cloud distribution is varying.

Simulation models in the design for energy-efficient buildings are developed to support research into model-based controls, system integration, energy management, and financial evaluation during the design phase (Hu and Karava, 2014). Effective simulation tools capable of predicting system behavior provided from the previously unobserved condition will allow the designer to make changes to system or activity while evaluating the effect of system behavior and performance concurrently (Coakley et al. 2014). For the simulation tool to be useful for research, significant levels of accuracy are needed (Royapoor and Roskilly, 2015).

The efficiency of the photovoltaic module is highly dependent on climatic conditions where the electricity output is determined by the sun's direction and sky condition during each day. It is very important to gain a better understanding of the inconsistencies of solar irradiance especially in countries in the tropical region where the cloud movement is high in variability. The goal of this paper is to observe the solar radiation incident on a vertical plane through long-term monitoring and to ascertain the most feasible vertical façade alignment for the PV system in Malaysia.

3. METHOD

3.1 EXPERIMENTAL SETUP AND SIMULATION CONFIGURATION

Eight main orientations were considered in this field measurement study. The devices were mounted vertically at a fixed inclination angle (90°) with eight distinct latitudes, representing north, north-east, east, south-east, south, south-west, west, and north-west. For this field analysis, the LP Pyra 08 Pyranometer from Delta Ohm used to determine the amount of incident solar irradiation from each horizontal façade of the PV module. LP Pyra 08 determines the amount of direct solar insolation and diffused flat surface irradiance in Watt/m^2. The pyranometer on each test unit was installed on a steel plate located in line with the module surface, on the side of the vertical surface, and between half of the surface's height, 1600mm from the ground. The placement of this

pyranometer is based on the outdoor Test Reference Environment established by the Joint Research Centre (JRC), European Commission for double skin façade application of BIPV (Bloem et al. 2012). Eight pyranometers were installed on 8 test units, which represents eight different azimuth angles. Figure 1 displays the structure diagram for the pyranometer and the data logger.

The shading effect can reduce the incoming solar radiation on the measurement device. The position of this experiment has to be in the plane field with no neighboring human and natural-made structure that would create shade to the measurement device over the entire experimental time. Also, the shadow was avoided from the measuring equipment and the mounting structure.
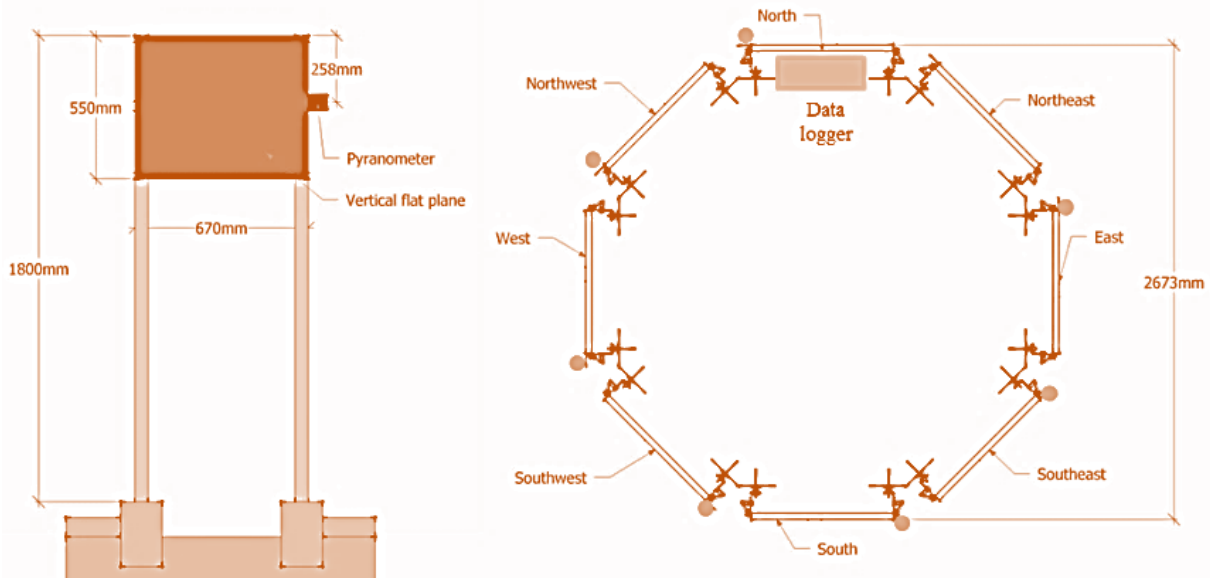
Figure 1: Instrumentation arrangement to measure incident solar radiation.

Based on the same instrumentation arrangement in the field test, the simulation process was undertaken using the System Advisor Model (SAM) created by the National Renewable Energy Laboratory (SAM, 2012).

Table 1: Kuala Lumpur's coordinates and annual climate condition

City	Kuala Lumpur
Time zone	GMT 8
Latitude	3.12 ^{o}N
Longitude	101.55 ^{o}E
Global horizontal	4.28 kWh/m^2/day
Direct normal (beam)	1.02 kWh/m^2/day
Diffuse horizontal	3.50 kWh/m^2/day
Average temperature	27.2 ^{o}C
Average wind speed	1.6 m/s

For this simulation, weather data from the US Department of Energy was used as it presents standard meteorological year data that are widely used in many building simulation programs. This climate data is in the format of IWEC (International Weather for Energy Calculations) produced by ASHRAE (American Society of Heating, Refrigerating, and Air-Conditioning Engineers) measured using an analytical system based on the sun-earth geometry, recorded cloud cover and temperature differences. The estimation for direct normal solar radiation depends on the sun angle and the ratio of global horizontal and total related extra-terrestrial solar radiation. This weather information includes hourly amounts for mean and long-term measurements over normal years. Table 1 displays

Kuala Lumpur's latitude and longitude, and regular solar output from the climate data. Figure 2 indicates the global, beam and diffuse irradiance at Kuala Lumpur.
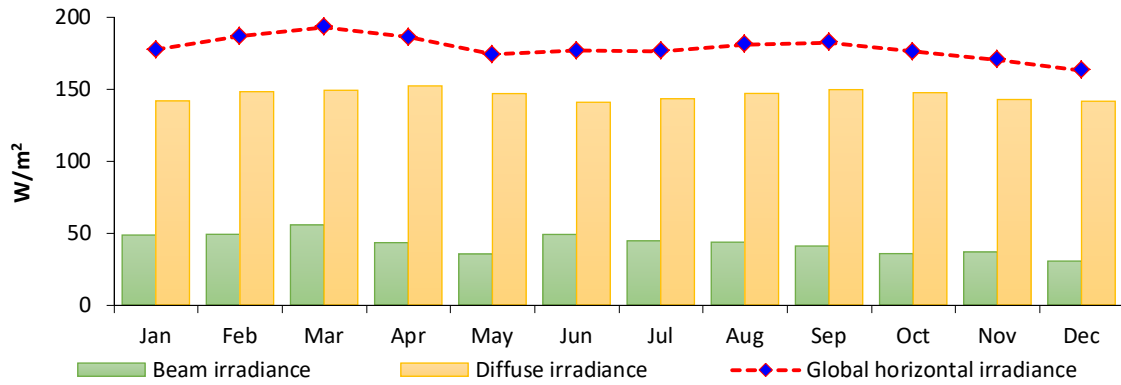
Figure 2: Average hourly global, beam, and diffuse irradiance according to a month in Kuala Lumpur.

3.2   VALIDATION METHOD BETWEEN SIMULATION ANS EXPERIMENTAL STUDY

Refsgaard (1997) relates to the validation model or prediction steps as a method to demonstrate that a specific site, numerical simulation able to make a precise simulation. The process of accepting, refusing, or qualifying the model, the result must be identified and documented well before the assessment begins (US EPA, 2002). The basic percentage of different calculations frequently resulted in an effect of restitution, whereby over-estimates canceled under-evaluations (Coakley et al. 2014). The introduction of structured statistical indices would provide a clearer model of results (Bou-Saada and Haberl, 1994).

3.2.1   NASH-SUTCLIFFE EFFICIENCY (NSE)

The NSE assessment model is the most common statistical model with comprehensive details on the values obtained (Servat and Dezetter, 1991) and the suggested use by the American Society of Civil Engineers (ASCE) (Legates and McCabe, 1999). The NSE standardized the statistic which calculated the relative significance of the residual variance and correlated the variation in the data measured (Nash and Sutcliffe, 1970). The variance standardization of the observation sequence results in a fairly higher NSE value. The NSE value ranges between ∞ to 1.0, where NSE=1 is perceived to be an ideal value corresponding to the model's good fit to the observed results. NSE = 0 specified that the prediction model is as precise as the average of the data observed. NSE = 0.0 to 1.0 can be seen as acceptable performance levels and NSE $<$ 0.0 specified that the average value observed is a good predictor that the simulated value, indicating inappropriate output (Moriasi et al. 2007). The NSE equation is given as

$$NSE = 1 - \left[\frac{\sum_{i=1}^{n}(Y_i^{obs} - Y_i^{sim})^2}{\sum_{i=1}^{n}(Y_i^{obs} - Y^{mean})^2} \right] \tag{1},$$

where, Y_i^{obs}, the ith observation for the constituent being evaluated. Y_i^{sim} , the ith simulated value for the constituent being evaluated. Y^{mean}, the mean of observed data for the constituent being evaluated. n, the total number of observations.

3.2.2   THE PERCENT BIAS (PBIAS)

The disparity between approaches referred to as the median of paired variations, which shows that the average one approach appears to underestimate or overstate the measurements of the second approach (Bartlett and Frost, 2008). The bias assessment tests the average propensity of the

simulated component value to be greater or lesser than the observed data and to indicate poor accuracy of the model (Gupta et al. 1999). The PBIAS approach is considered when aiming to evaluate a split-sample assessment (Moriasi et al. 2007). ASCE also suggests the PBIAS method. The PBIAS values are in percentage where, PBIAS = 0 indicates the accuracy of the model simulation data (optimal value), while PBIAS equivalent to positive value indicates the model underestimates bias and overestimates bias when negative PBIAS values. The PBIAS equation is

$$PBIAS = \left[\frac{\sum_{i=1}^{n}(Y_i^{obs} - Y_i^{sim})*100}{\sum_{i=1}^{n} Y_i^{obs}} \right] \tag{2},$$

where, Y_i^{obs}, the ith observation for the constituent being evaluated. Y_i^{sim}, the ith simulated value for the constituent being evaluated. n, the total number of observations.

3.2.3 ROOT MEAN SQUARE ERROR (RMSE) – OBSERVATION STANDARD DEVIATION RATIO (RSR)

To determine the accuracy of the prediction simulation model, the relative output measurement on the dataset must be considered. There are several other reliability metrics frequently used in model assessments. Which included Mean Absolute Error (MAE), Mean Square Error (MSE), and Root Mean Square Error (RMSE). The method of measurement is often named the performance metrics and the error-index (Cao and Tay, 2003). The outcome of these performance indicators is important as it provides the error in the units of the constituent of consideration which helps in the analysis of the results (Moriasi et al. 2007). Often known as Mean Absolute Deviation (MAD), the Mean Absolute Error (MAE) calculates the average absolute deviation of the predicted value from the measured data (Adhikari and Agrawal, 2013). MAE indicates the amount of total error due to forecasting without taking into account the direction of error, and the lower MAE value shows a strong forecast. The formula to calculate the MAE is:

$$MAE = \frac{1}{n} \sum_{i=1}^{n} |Y_i^{obs} - Y_i^{sim}| \tag{3},$$

where, Y_i^{obs} is the ith observation for the constituent being evaluated. Y_i^{sim} is the ith simulated value for the constituent being evaluated. n, the total number of observations.

Root Mean Square Error (RMSE) is among the most widely used error-index indicator evaluating the average inaccuracy (Chu and Shirmohammadi, 2004; Singh et al. 2004; Vasquez-Amabile and Engel, 2005). RMSE demonstrates the discrepancy between predicted and respective measured data in-square before average (Adhikari and Agrawal, 2013). If the RMSE and MAE values are less than half the SD of the measurement values, it may be considered small, and either is acceptable for model assessment (Singh et al.. 2004). The RMSE formula is given as

$$RMSE = \sqrt{\frac{1}{n} \sum_{i=1}^{n} (Y_i^{obs} - Y_i^{sim})^2} \tag{4},$$

where, Y_i^{obs} is the ith observation for the constituent being evaluated. Y_i^{sim} is the ith simulated value for the constituent being evaluated. n, the total number of observations.

Sing et al. also produced the simplified RMSE model using standard observation deviation, adding the error-index and additional details. Moriasi et al. (2007) suggest that the RSR output metrics combine the advantages of the error-index statistics and have a scaling/normalization

component where the result value can be extended to the different constituents. The value of the RSR ranges from an ideal value of 0, which implies zero RMSE or residual variance, and thus optimal model simulation to a great positive value. The lesser the RSR value, the better the performance of the simulation model. This technique has known the RMSE-Observations Standard Deviation Ratio (RSR) and RSR measurement is written as

$$RSR = \frac{RMSE}{STDEV_{obs}} = \frac{\sqrt{\sum_{i=1}^{n}(Y_i^{obs} - Y_i^{sim})^2}}{\sqrt{\sum_{i=1}^{n}(Y_i^{obs} - Y^{mean})^2}}$$ (5),

where, Y_i^{obs} is the ith observation for the constituent being evaluated. Y_i^{sim} is the ith simulated value for the constituent being evaluated. Y^{mean} is the mean of observation value over n. n is the total number of observations.

4. RESULT AND DISCUSSION

4.1 FIELD TEST ANALYSIS

This section analyzed the incident solar radiation based on eight different latitude angles, on eight horizontal facades. Six months of solar radiation data can be obtained from the field measurement analysis due to limited time and required equipment. In this observational study, the analysis was considered for 12 hours of the daytime period between 7.00-19.00 hr., as well as the interval duration of two minutes of data obtained from the pyranometer. Figure 3 illustrates the November 2015 average hourly incident irradiance, and Figure 4 shows the frequency percentage of the irradiance level during the day. For the north and south façade, the hourly trend of incident solar radiation is nearly identical during the day, gradually increasing from morning to peak around noon, and decreasing towards evening.
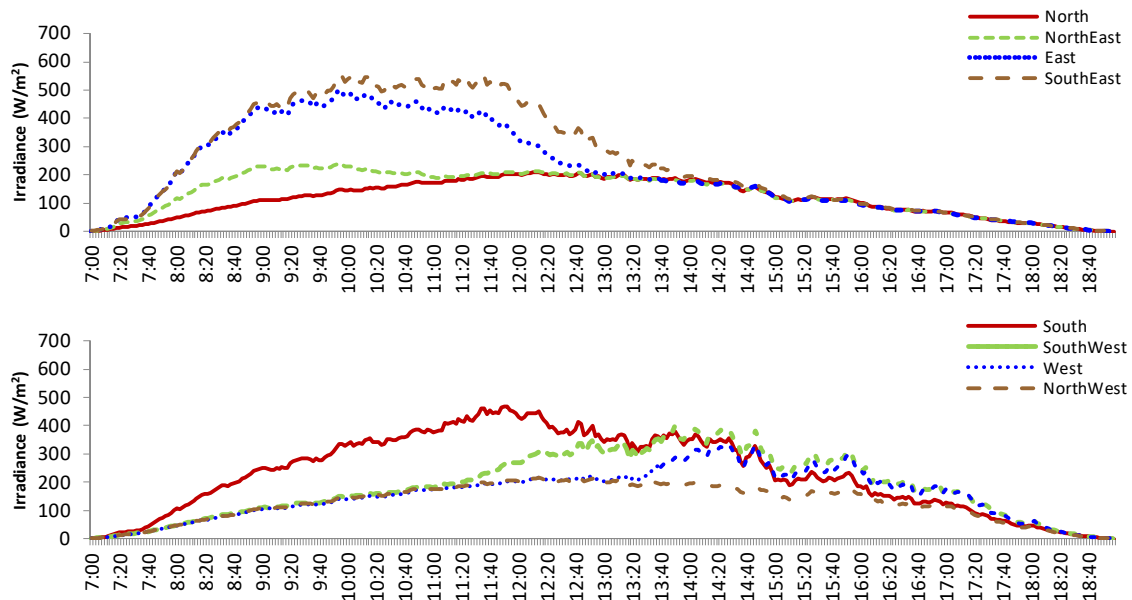
Figure 3: Average hourly observation of incident solar radiation in November 2015

In the meantime, the south façade obtained an irradiance amount of about 40% from 300 to 500W/m². The northeast, east, and south-east horizontal plane recorded a higher degree of irradiance varying peak periods during morning hours; northeast at 9.00 a.m., east at 9.30 a.m. and south-east at 11.00 a.m. The south-east façade had an irradiance level of approximately 16.7% between 500-600W/m². Meanwhile during the evening period, the south-west, west, and north-west

horizontal plane received higher levels of irradiance.
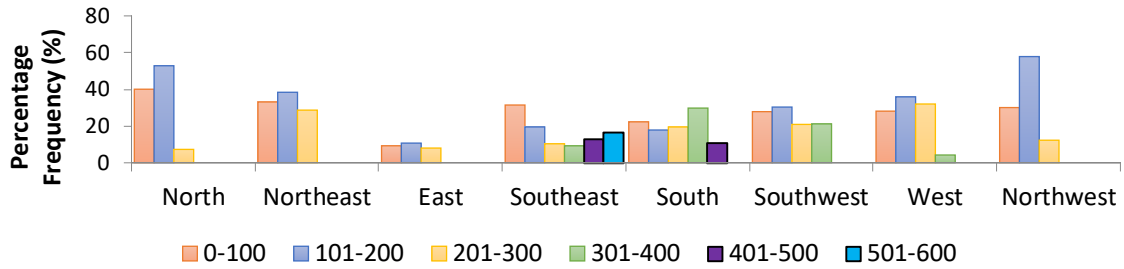
Figure 4: Hourly percentage frequency of incident solar radiation in November 2015.

The same trend also occurred in December 2015. Figure 5 and Figure 6 display the average hourly and percentage of the incident solar radiation in December. North, northeast, and northwest irradiance level was below $200W/m^2$. Approximately 28.6% of the amount of irradiance on the east façade was above $300W/m^2$ while 9.7% on the west. However, on the south-east horizontal plane, about 15% of the irradiance level was between $500-700W/m^2$.
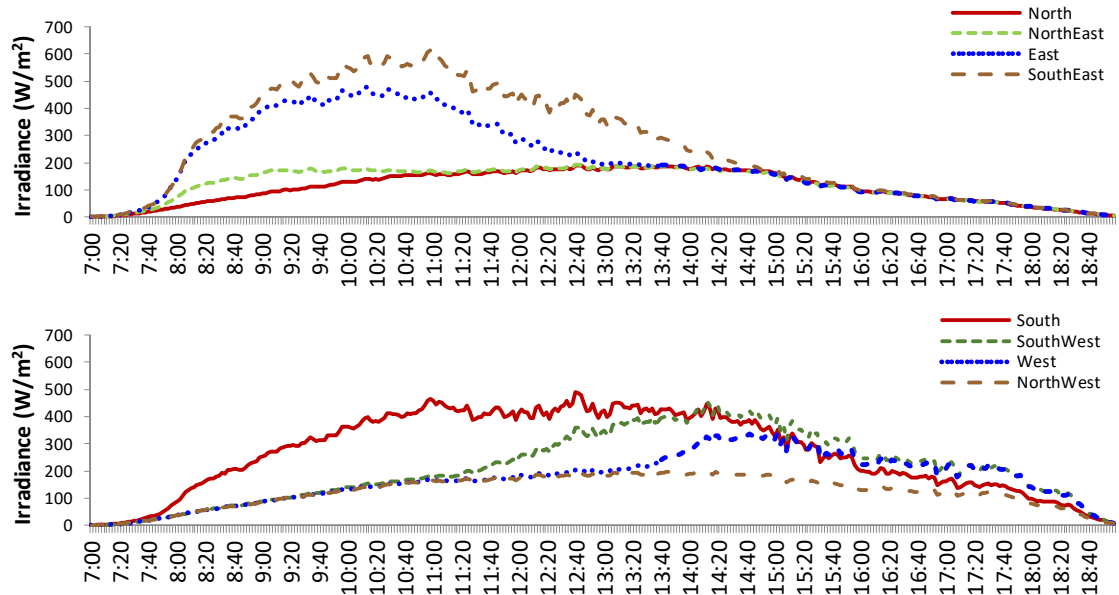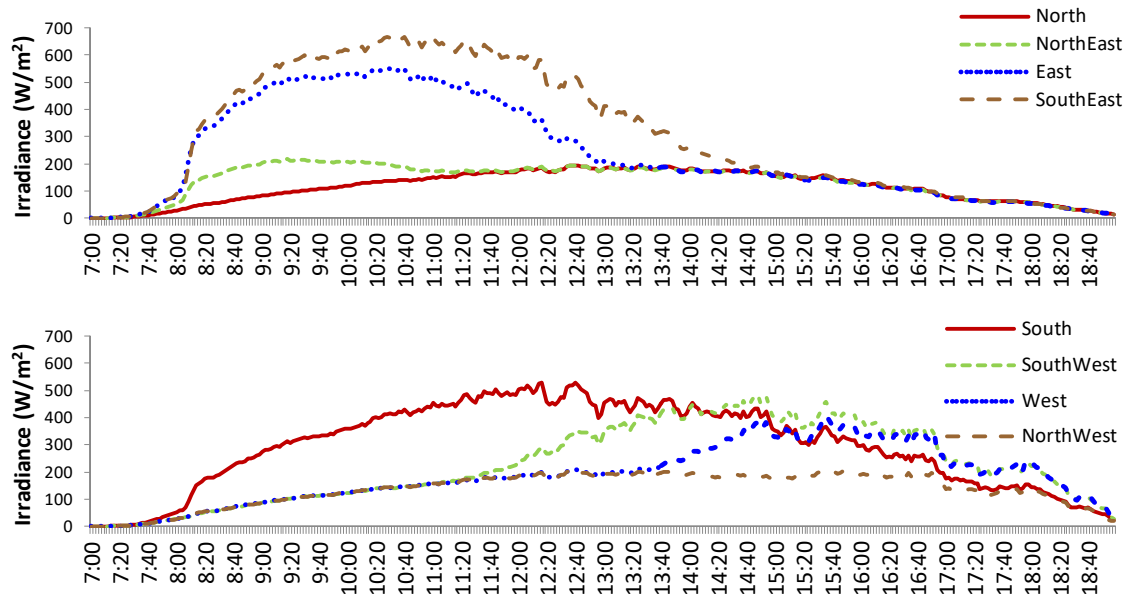

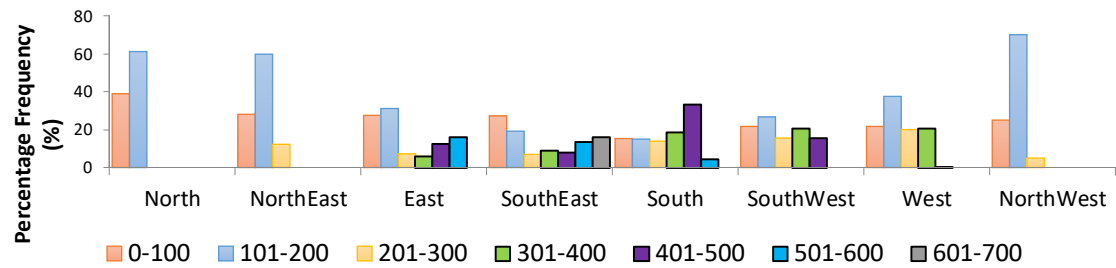**Figure 5**: Hourly analysis of incident solar radiation in December 2015
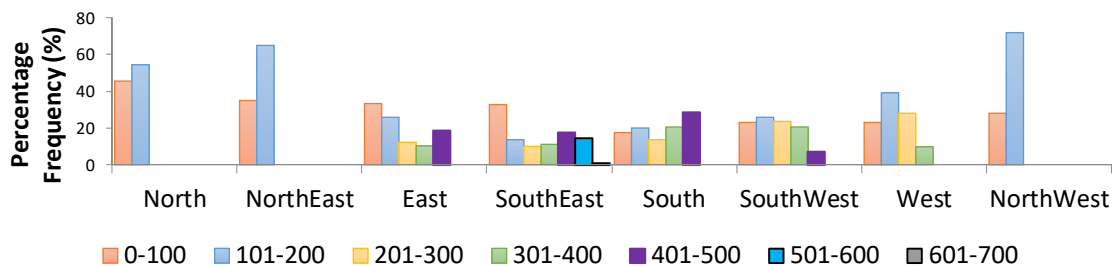
Figure 6: Hourly percentage frequency of incident solar radiation in December 2015

The highest incident irradiance reported in January between 10.00 a.m to noon on the south-east façade. The irradiance level ranges between $600-700W/m^2$ are 16.1%. The second highest was on the east façade between 9:00-11:00 a.m. with a 15.8% irradiance level ranges $500-600W/m^2$. Whereas, for other vertical plane orientations, the average irradiance level is below $500W/m^2$ during January, with the north façade remaining low on incident solar radiation. Figures 7 and 8 display the January average hourly and percentage level on the vertical incident solar irradiance.
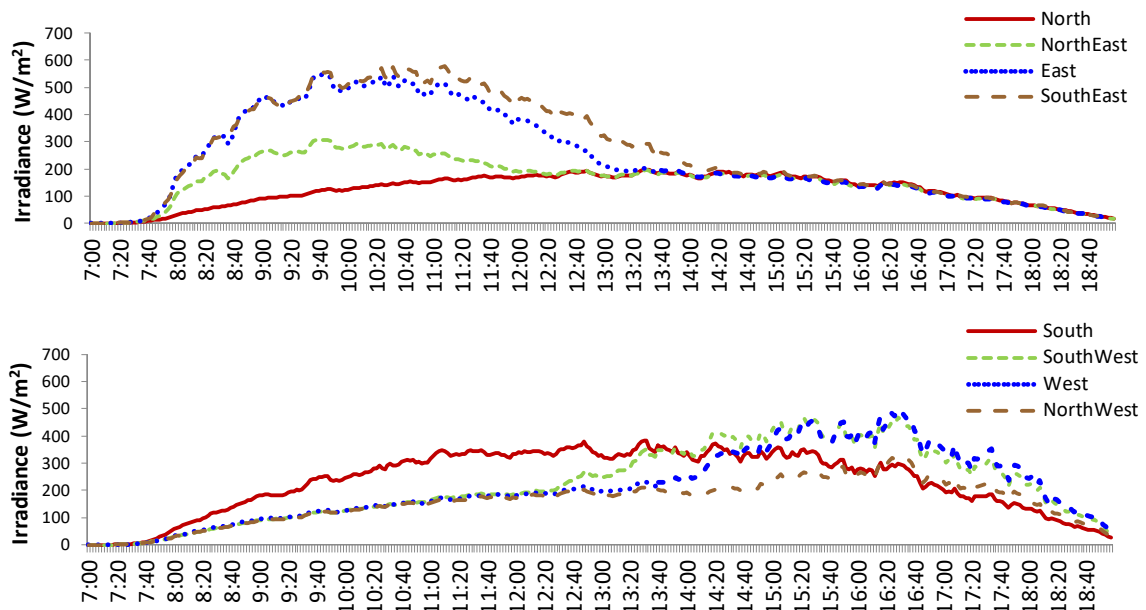
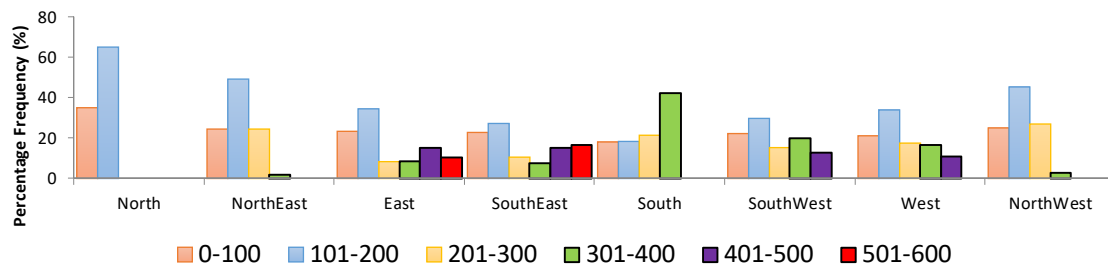**Figure 7**: Hourly analysis of incident solar radiation in January 2016.

Figure 8: Hourly percentage frequency of incident solar radiation in January 2016

The average incident solar radiation level on all vertical façade, however, is below 600W/m² in February. During this month's morning hours, 16.7% and 10.6% of the irradiance rates reported on the south-east and east facades were between 500-600W/m². The south-west and west façade displayed higher irradiance levels for 15:00-16:40 with 12.8%, and 10.8% irradiance level is 400-500W/m². Other façade orientations, see Figures 9 and 10, remain below 400W/m².

Figure 9: Hourly analysis of incident solar radiation in February 2016.

Azhar Ghazali, Lim Chin Haw

Figure 10: Hourly percentage frequency of incident solar radiation in February 2016.

In the morning and evening hours of March, the average hourly incident solar radiation on the east and west vertical orientation displayed higher measurement. From 9:20 a.m. until 10:20 am, the east façade recorded about 7% incident irradiance in the range between 600-700W/m^2. Meanwhile, from 15.30 to 16.30 the western façade earned the maximum, with an irradiance between 500-600W/m^2. Throughout the day, however, the morning period irradiance level is higher than the evening period. Figure 11 and Figure 12 indicate the March average hourly and percentage frequency of vertical incident solar radiation.
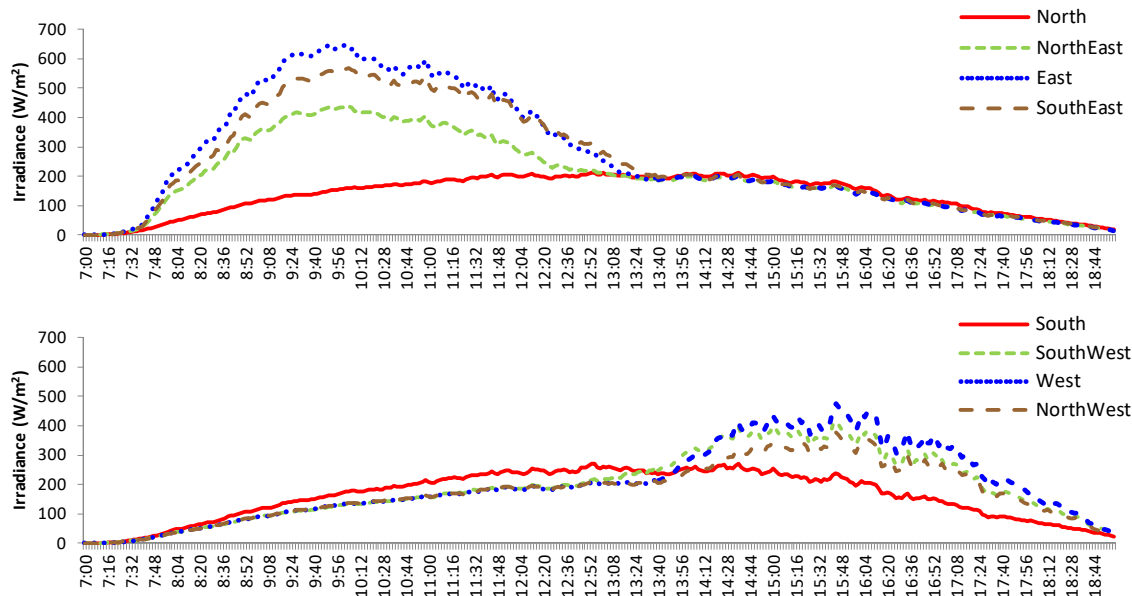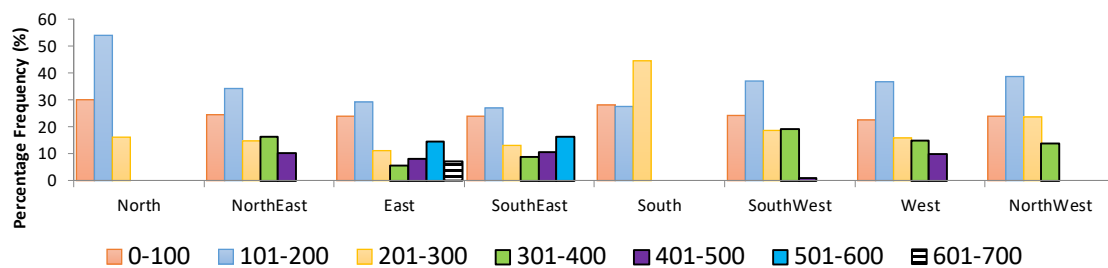

Figure 11: Hourly analysis of incident solar radiation in March 2016.

Figure 12: Hourly percentage frequency of incident solar radiation in March 2016

A certain pattern happened in April as well. In the morning duration northeast, east and south-east façade recorded the highest incident solar radiation, with a peak about 10.00 am and gradually decline towards midday. Meanwhile, the incident irradiance amount has gradually increased towards noon on the southeast, west, and northeast. Around 13.00 the irradiance level on this façade has risen and reached its peak at about 15.00. Figure 13 and Figure 14 indicates the April average

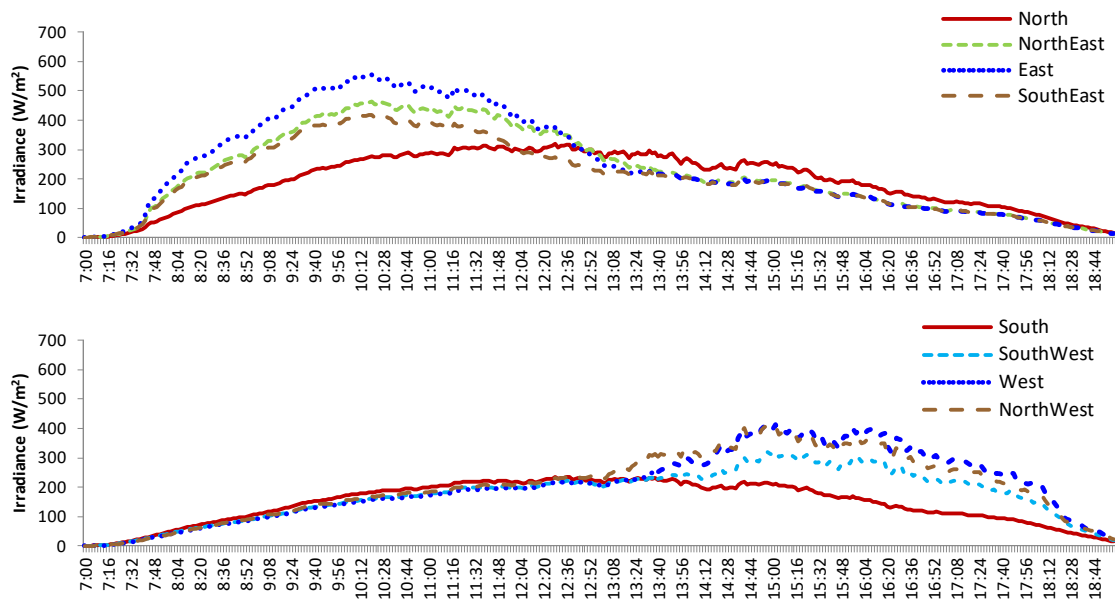hourly and percentage level of the vertical incident solar radiation

Figure 13: Hourly analysis of incident solar radiation in April 2016.
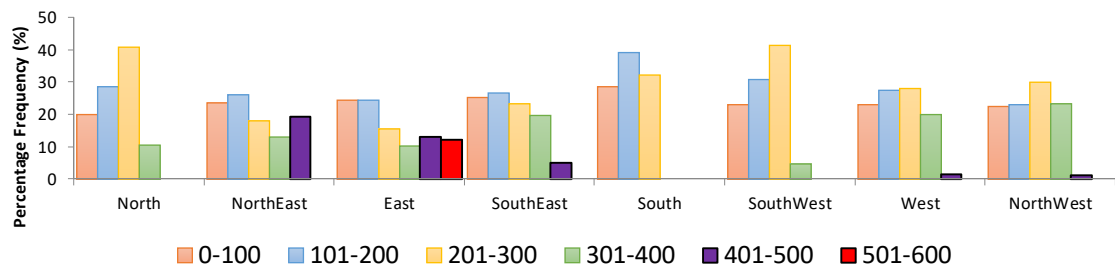

Figure 14: Hourly percentage frequency of incident solar radiation in April 2016

Figure 15 shows the mean irradiance per month. The south-east façade received the maximum incident irradiance with a mean value of 248W/m^2 in November, followed by 233W/m^2 and 213W/m^2 (respectively) on the south and east façade. The highest mean incident irradiance recorded in December was on the southern façade with 270 W/m^2 followed by southeastern and southwestern façade with 263W/m^2 and 208W/m^2 (respectively). The North façade remained the lowest obtained incident irradiance. Meanwhile, the highest reading was observed with 304W/m^2 on the south-east façade in January, followed by 296W/m^2 and 227W/m^2 on the south and south-west façade. The south-east façade also recorded the highest incident solar radiation in February compared to another with an average of 264W/m^2 and then the north (239W/m^2) and south (235W/m^2) followed.

Meanwhile in March, as the declination angle of the sun in the equatorial region is almost 0°, the eastern façade obtained the highest mean incident solar radiation compared to another vertical façade with 267W/m^2, followed by south-east, northeast and west façade with 251W/m^2, 203W/m^2, 199W/m^2 (respectively). However, with 135W/m^2 and 162W/m^2 the lowest mean incident irradiance obtained by the north and south facades. The sun position is marginally on Malaysia's northern side in April; the southern vertical façade recorded the lowest mean incident solar radiation compared to another façade with 146W/m^2 while irradiance on the northern façade has risen to 190W/m^2. Morning sunlight led to an increase in the east and northeast facades receiving the highest mean with 248W/m^2 and 226W/m^2 of incident solar radiation. Table 2 gives the summary of mean vertical incident solar radiation over six months.
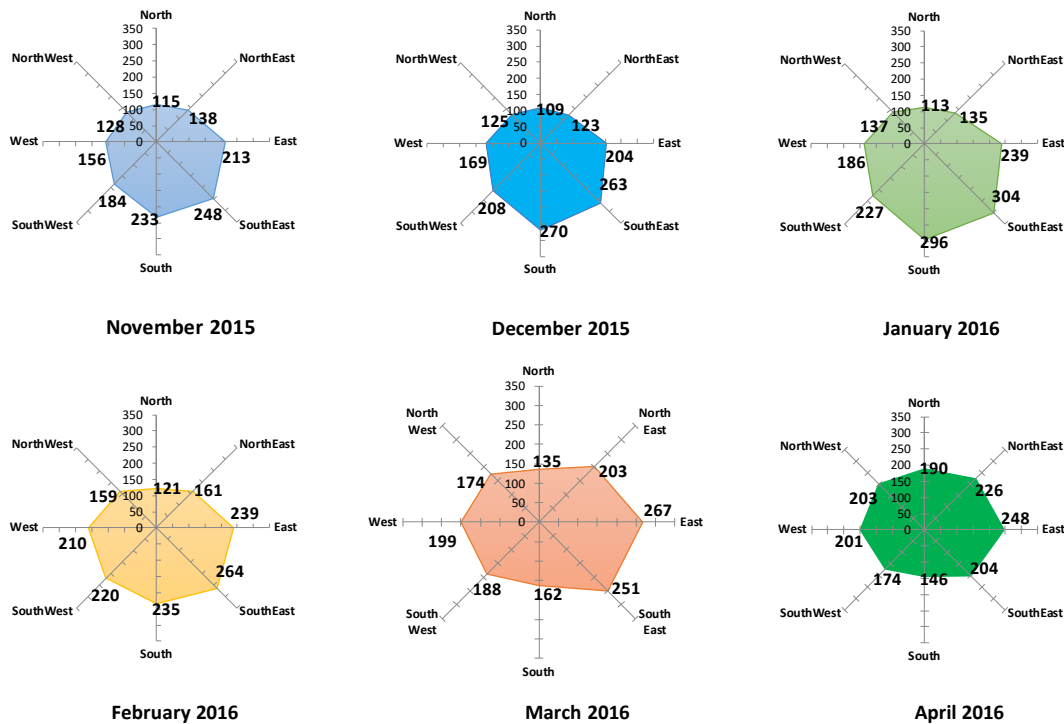
Azhar Ghazali, Lim Chin Haw

Figure 15: Mean incident irradiance according to month.

Table 2: Summary of mean incident irradiance of 8 façade orientation in six months.

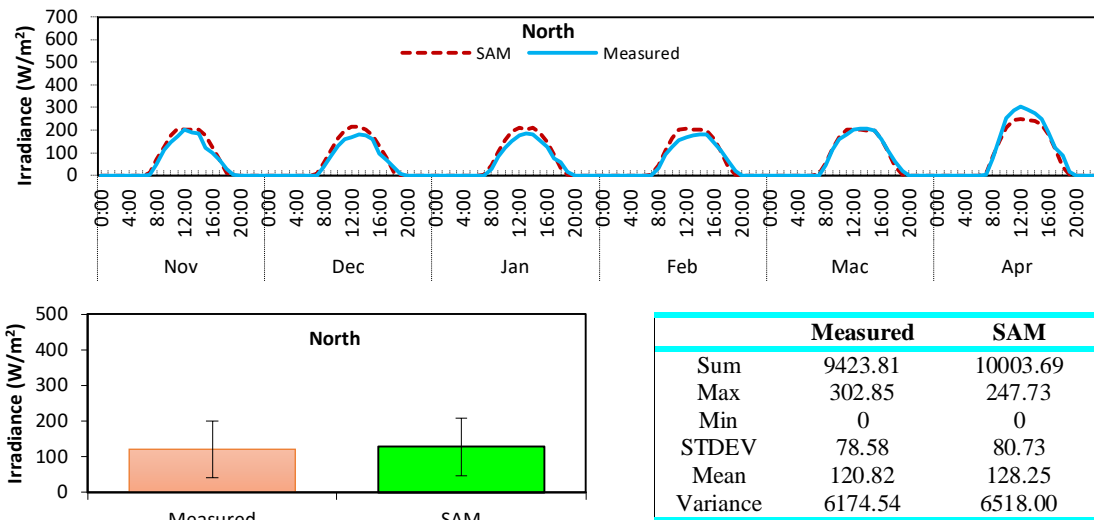| Façade Orientation	North	Northeast	East	Southeast	South	Southwest	West	Northwest
Nov-15	115	138	213	248	233	184	156	128
Dec-15	109	123	204	263	270	208	169	125
Jan-16	113	135	239	304	296	227	186	137
Feb-16	121	161	239	264	235	220	210	159
Mar-16	135	203	267	251	162	188	199	174
Apr-16	190	226	248	204	146	174	201	203

4.2 VALIDATION ANALYSIS

Predicated on the hourly result, it can prove that the pattern of incident solar radiation is about the same on each vertical façade, where the vertical north and south reaches the high point at midday between 13.00-14.00. During the morning time, the northeastern, eastern and southeastern façade display higher irradiance while southwestern, western, and northwestern façade in the evening period.
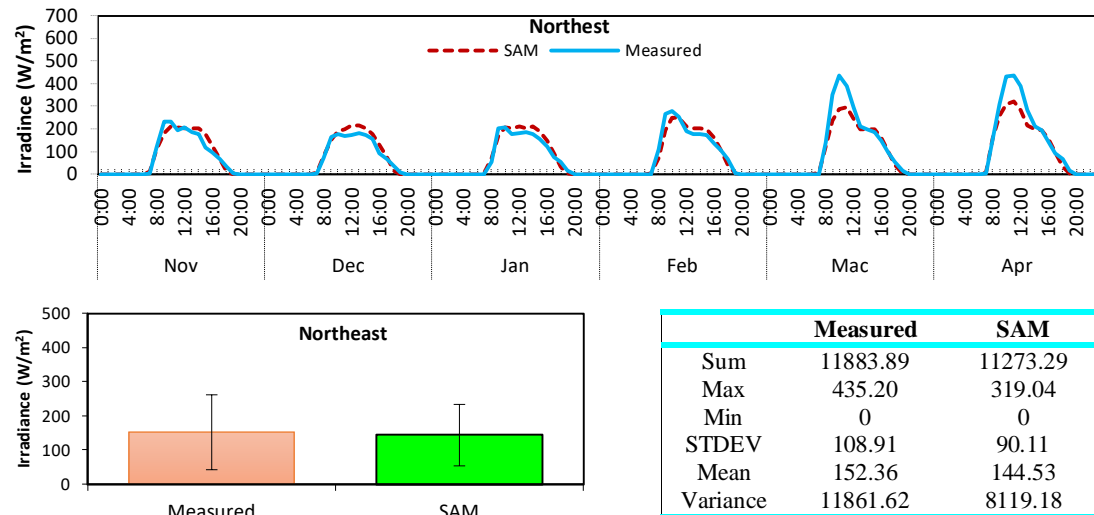
On the northern façade, the simulation average data is higher than on the field test data. Whereas the measured data showed higher irradiance compared to the simulation data. The mean variation in the east, south-east and south façade is greater while the north-east, southwest, west, and north-west façade are smaller. In Figure 16 to Figure 23 below, this result can be seen in the mean and standard deviation error bar on each façade configuration.

Table 3: Forecast/error indicator between measured and simulated data of incident irradiance on each vertical orientation

Forecast/error indicator	N	NE	E	SE	S	SW	W	NW
NSE	0.90	0.86	0.72	0.70	0.85	0.84	0.78	0.82
PBIAS	-6.15	5.14	22.34	25.80	16.79	7.35	4.51	0.24
MAE	20.75	27.28	61.75	68.91	39.98	37.58	39.62	29.61
MSE	635.02	1668.33	8835.76	11280.55	2960.41	2582.29	3034.73	1536.75
RMSE	25.20	40.85	94.00	106.21	54.41	50.82	55.09	39.20
STDEV	6095.38	11709.55	31566.31	37084.07	19288.4	15707.23	13573.21	8499.29
RSTDEV	78.07	108.21	177.67	192.57	138.88	125.33	116.50	92.19
RSR	0.32	0.38	0.53	0.55	0.39	0.41	0.47	0.43

Figure 16: Hourly measured and simulated incident irradiance on the North facade.

	Measured	SAM
Sum	9423.81	10003.69
Max	302.85	247.73
Min	0	0
STDEV	78.58	80.73
Mean	120.82	128.25
Variance	6174.54	6518.00

Figure 17: Hourly measured and simulated incident irradiance on the Northeast façade.

	Measured	SAM
Sum	11883.89	11273.29
Max	435.20	319.04
Min	0	0
STDEV	108.91	90.11
Mean	152.36	144.53
Variance	11861.62	8119.18
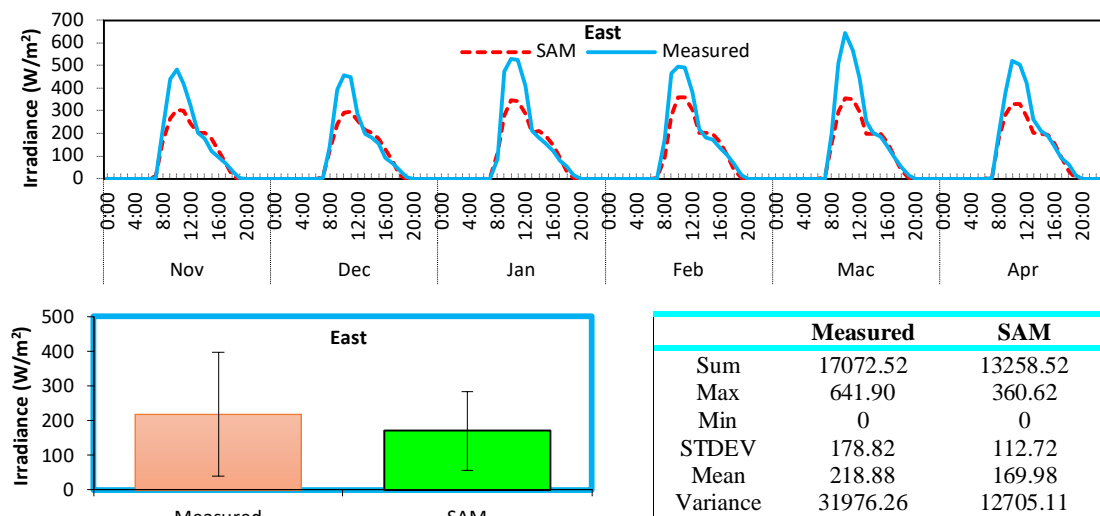
Figure 18: Hourly measured and simulated incident irradiance on East facade.

	Measured	SAM
Sum	17072.52	13258.52
Max	641.90	360.62
Min	0	0
STDEV	178.82	112.72
Mean	218.88	169.98
Variance	31976.26	12705.11
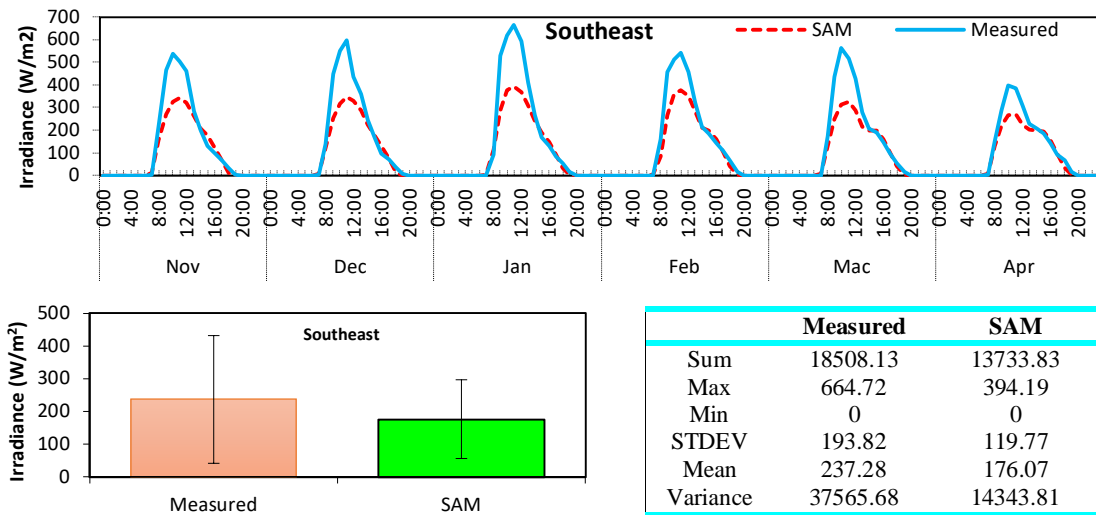
Figure 19: Hourly measured and simulated incident irradiance on Southeast facade

	Measured	SAM
Sum	18508.13	13733.83
Max	664.72	394.19
Min	0	0
STDEV	193.82	119.77
Mean	237.28	176.07
Variance	37565.68	14343.81
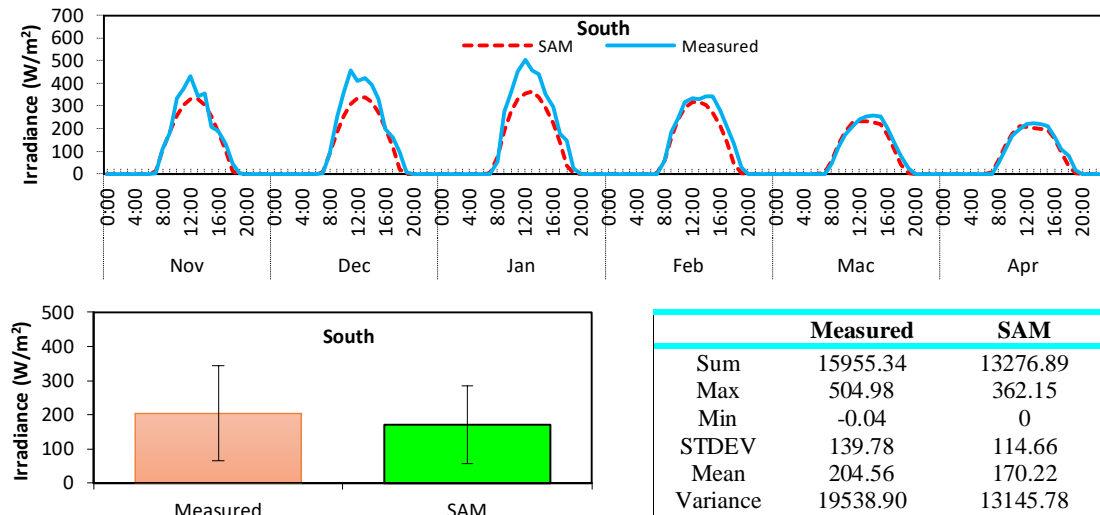
Figure 20: Hourly measured and simulated incident irradiance on the South façade

	Measured	SAM
Sum	15955.34	13276.89
Max	504.98	362.15
Min	-0.04	0
STDEV	139.78	114.66
Mean	204.56	170.22
Variance	19538.90	13145.78
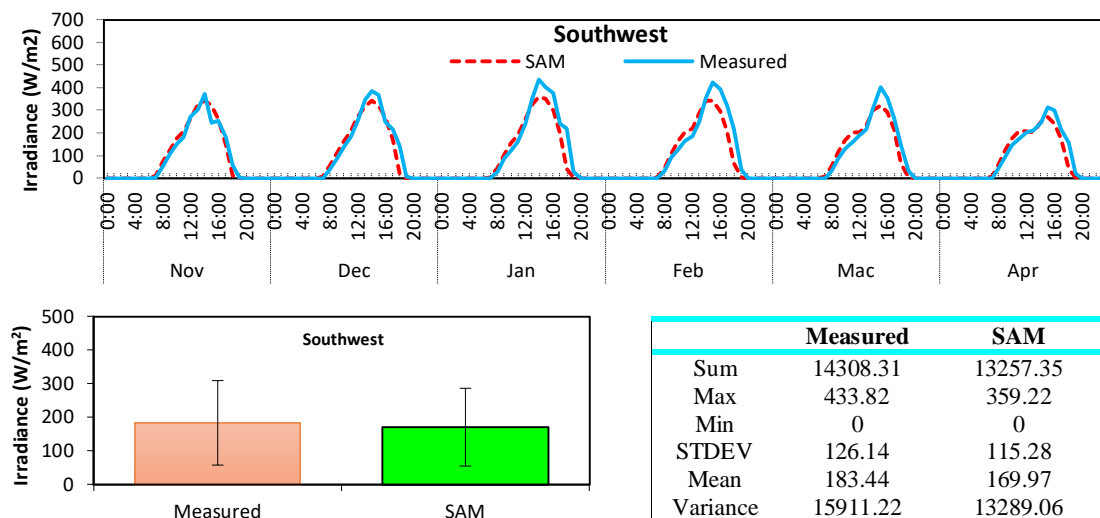
Figure 21: Hourly measured and simulated incident irradiance on the Southwest facade.

	Measured	SAM
Sum	14308.31	13257.35
Max	433.82	359.22
Min	0	0
STDEV	126.14	115.28
Mean	183.44	169.97
Variance	15911.22	13289.06

13
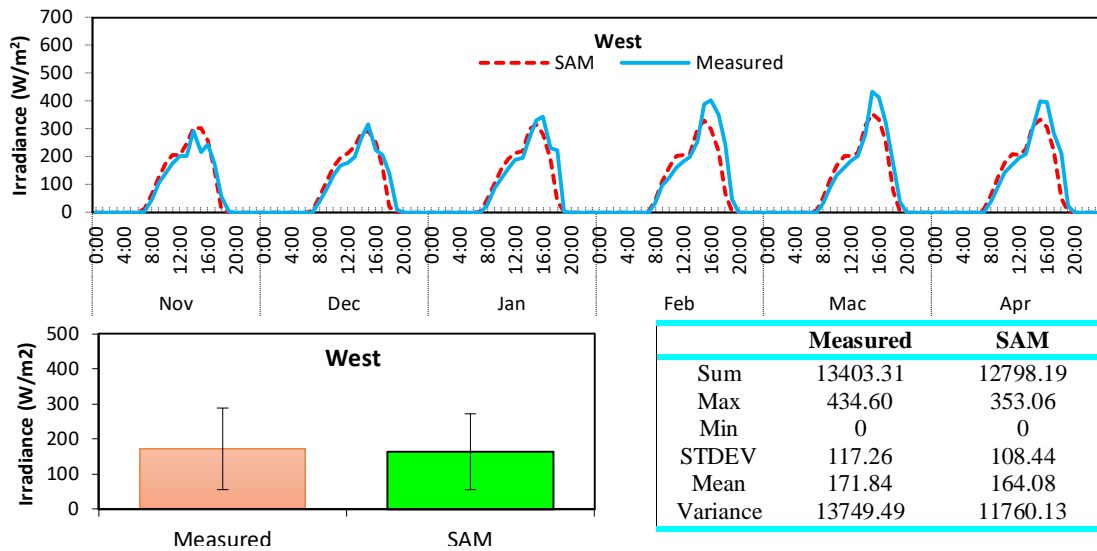
Figure 22: Hourly measured and simulated incident irradiance on the West facade

	Measured	SAM
Sum	13403.31	12798.19
Max	434.60	353.06
Min	0	0
STDEV	117.26	108.44
Mean	171.84	164.08
Variance	13749.49	11760.13
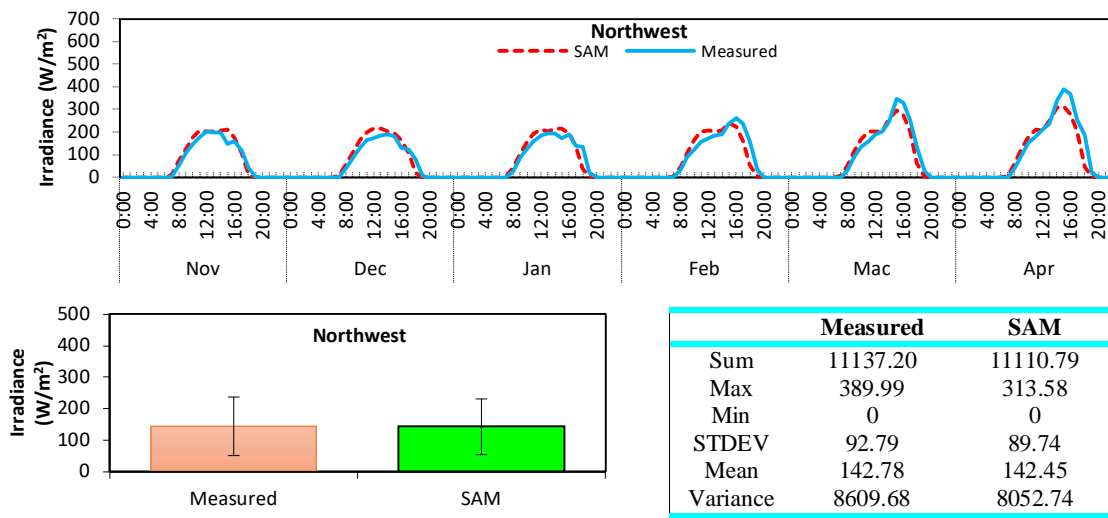
Figure 23: Hourly measured and simulated incident irradiance on the Northwest facade.

	Measured	SAM
Sum	11137.20	11110.79
Max	389.99	313.58
Min	0	0
STDEV	92.79	89.74
Mean	142.78	142.45
Variance	8609.68	8052.74

Table 3 shows the results of the statistical method of validation analysis between the measured and simulated data. The Nash-Sutcliffe Efficiency (NSE) indicator indicates the difference between the data and the simulation data are below the appropriate range of 0.7 but near to the ideal value of 1. The bias comparison of the simulation data to measured data using PBIAS showed that the simulated data had overestimated the irradiance of almost 6.15% on the northern façade, whereas SAM has underestimated the data on other orientations. SAM has underestimated the eastern and southeastern façade approximately between 22% to 25%, but in the northwestern façade, the percentage bias is 0.25% which is close to the ideal value of 0%.

Additionally, the simulation data error-index based on the MSE indicator showed that the value of each façade orientation is less than half of the STDEV value, suggesting that the simulated data is a suitable model for this study. The standardized RMSE to Observation Standard Deviation Ratio showed that in every façade configuration the error in simulation is relatively small with RSR of 0.55. This result suggests that the computed incident irradiance in the SAM simulation model is nearly fit to the observed data in the field measurement.

4.3 ANNUAL INCIDENT IRRADIANCE ON VERTICAL FACADE

The simulation analysis in SAM based on the same specification continued to evaluate which vertical façade orientation obtained the highest incident solar radiation in one year under Malaysian climatic conditions. The result indicates that the eastern façade obtained the highest mean daily solar radiation at $168.9W/m^2$ followed by the western façade at $163.7W/m^2$, see Figure 24. Whereas, with $144W/m^2$ and $150W/m^2$, the northern and southern façade obtained the lowest incident irradiance. Table 4 presented the average daily incident irradiance based on SAM analysis for each façade alignment.
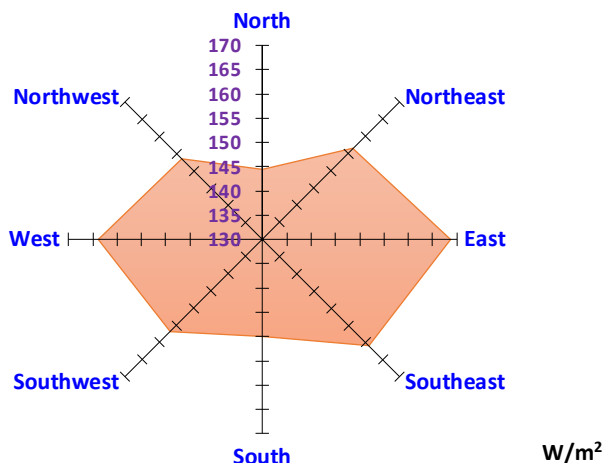

Figure 24: Mean daily incident irradiance (simulated)

Table 4: Summary of mean daily incident irradiance on each orientation.

	N	NE	E	SE	S	SW	W	NW
Mean Daily	144.45	156.45	168.79	161.01	150.06	156.85	163.74	153.48
STDEV	93.2	101.6	112.5	108.8	102.0	104.1	107.7	100.1

5. CONCLUSION

Based on the field measurement of incident irradiance on vertical façade orientation in Malaysia, the northern and southern façade received the least incident irradiance throughout the analysis period and reached its highest irradiance level during the noon period. During the morning period North, Northeast, and East vertical façade received higher incident irradiance, while South, Southwest, and West are during the evening period.

The forecast or error indicator between field measurement data and simulated data have shown that the incident solar radiation on the vertical façade calculated by the System Advisor Model is almost fit for the field measurement data. Thus, based on SAM analysis of yearly incident irradiance on vertical façade in Malaysia, East, West, Southeast, and Southwest orientation received the highest mean irradiance compared to another vertical facade. The finding indicates that building façade for these orientations has better energy output for vertical PV applications in Malaysia's climate condition.

6. AVAILABILITY OF DATA AND MATERIAL

Data can be made available by contacting the corresponding author.

7. REFERENCES

Adhikari R and Agrawal R K (2013). An Introductory Study on Time Series Modelling and Forecasting, Germany, LAP LAMBERT Academic Publishing

Bartlett, J.W. and Frost, C. (2008). Reliability, repeatability, and reproducibility: analysis of measurement errors in continuous variables. *Ultrasound Obstet Gynecol.* 31: 466-475.

Bloem, J.J., Lodi, C., Cipriano, J., Chemisana, D. (2012). An outdoor test reference environment for double skin application of building integrated photovoltaic system. *Energy and Building* 50: 63-73.

Bou-Saada, TE, Haberl JS. An improved procedure for developing calibrated hourly simulation models. In: Proceedings of the 5th international IBPSA conference. Montréal, Canada; 1995

Cao, L.J and Tay, F.E.H 2003 Support Vector Machine with Adaptive Parameters in Financial Time Series Forecasting. In: IEEE Transaction on Neural Networks, 14(6), 1506-1518

Chu, T. W., and A. Shirmohammadi. (2004). Evaluation of the SWAT model's hydrology component in the piedmont physiographic region of Maryland. Trans. ASAE 47(4): 1057-1073.

Coakley, D., Raftery, P., and Keane, M. (2014). A review of methods to match building energy simulation models to measured data. Renewable and Sustainable Energy Reviews. 37: 123-141.

Denholm, P., and Margolis, R. (2007). Evaluating the limits of solar photovoltaics (PV) in traditional electric power systems. *Energy Policy*. vol. 35, 2007.

Espinar, B., Aznerte, J.L., Girard, R., Moussa, A.M., Karinio-Takis, G. (2010). Photovoltaic Forecasting: A state of the art. 5th European PV-Hybrid and Mini-Grid Conference, Apr 2010, Tarragona, Spain. OTTI - Ostbayerisches Technologie-Transfer-Institut, 250-255.

Gupta, H. V., S. Sorooshian, and P. O. Yapo. 1999. Status of automatic calibration for hydrologic models: Comparison with multilevel expert calibration. J. Hydrologic Eng. 4(2), 135-143.

Hu, J., and Karava, P. (2014). A state-space modeling approach and multi-level optimization algorithm for predictive control of multi-zone buildings with mixed-mode cooling. *Building and Environment*, 80, 259-273.

Janjai, S., and Deeyai, P. (2009). Comparison of methods for generating typical meteorological year using meteorological data from a typical environment. *Applied Energy* 85: 528-537

Legates, D.R. and McCabe, G. J. (1999) Evaluating the use of "goodness-of-fit" measures in hydrologic and hydroclimatic model validation. Water Resources Research. 35(1), 233-241.

Madhu, V., and Gangadharan, K. (2016). Temporal distribution of column ozone over Cochin – A study based on the in-situ measurement and ECMWF reanalysis. Scientific Research. 6(2): 11-20.

Markvart, T. (2002). *Photovoltaic Solar Energy Conversion*. European Summer University: Energy for Europe 2002. http://www.soton.ac.uk/~solar/files/Strasbourg.pdf.

Mayer, D., Wald, L., Poissant, Y., and Pelland, S. (2008). Performance prediction of grid-connected photovoltaic systems using remote sensing. Technical Report IEA-PVPS T2-07:2008, International Energy Agency - Photovoltaic Power Systems Programme (IEA - PVPS Task 2).

Mohanty, P., Muneer, T., Gago, E.J., Kotak, Y. 2015. Solar radiation fundamentals and PV system components. Solar Photovoltaic System Applications, *Green Energy, and Technology*, 7-47. Doi: 10.1007/978-3-319-14663-8_2

Moriasi, D.N., Arnold, J.G., Van Liew, M.W., Bingner, R.L., Harmel, R.D., Veith, T.L. (2007). Model evaluation guideline for systematic quantification of accuracy in watershed simulations. *American Society of Agricultural and Biological Engineers*. 50(3): 885-900.

Nash, J.E. and Sutcliffe, J.V. (1970) River flow forecasting through conceptual models: Part 1. A discussion of principles. *Journals of Hydrology*. 10(3), 282-290.

Nobre, A.M., Severiano, C.A., Karthik, S., Kubis, M., Zhao, L., Martins, F.R., Pereira, E.B., Reindl., T. 2016. PV power conversion and short-term forecasting in a tropical, densely built environment in Singapore. *Renewable Energy* 94: 496-509.

Ortega-Vazquez, M.A.; Kirschen, D.S. 2010 Assessing the impact of wind power generation on operating costs. *IEEE T. Smart Grids* 1: 295–301.

Servat, E., and Dezetter, A. 1991. Selection of calibration of objective functions in the context of rainfall-runoff modeling in a Sudanese savannah area. Hydrological Science Journal, 36(4), 307-330.

Refsgaard, J. C. (1997). Parameterisation, calibration, and validation of distributed hydrological models. *Journal of Hydrology*, 198(1): 69-97

Royapoor, M and Roskilly, T. (2015). Building model calibration using energy and environmental data. *Energy and Building*, 94: 109-120.

Singh, J., H. V. Knapp, and M. Demissie. (2004). Hydrologic modeling of the Iroquois River watershed using HSPF and SWAT. ISWS CR 2004-08. Champaign, Ill.: Illinois State Water Survey. http://www.sws.uiuc.edu/pubdoc/CR/ ISWSCR2004-08.pdf. Accessed September 2005.

SAM (2012). National Renewable Energy Laboratory. Golden, CO. System Advisor Model Version 2012.5.11 (SAM 2012.5.11)

US EPA. 2002. Guidance for quality assurance project plans for modeling. EPA QA/G-5M. Report EPA/240/R-02/007. Washington, D.C.: U.S. EPA, Office of Environmental Information.

WMO. (2012). Guide to meteorological instruments and methods of observation. World Meteorological Organization, WMO-No.8.

Dr. Muhamad Azhar Bin Ghazali is a Lecturer in Architecture at School of Housing, Building, and Planning, Universiti Sains Malaysia, Penang, Malaysia. His research emphasizes on Solar Radiation on Building, Building Integrated Photovoltaic (BIPV), Low-Carbon Building, Renewable Energy, Sustainable Building Design, Passive & Active Architecture.

Ar. Dr. Lim Chin Haw is a Senior Research Fellow at the Solar Energy Research Institute (SERI), University Kebangsaan Malaysia, and a Professional Registered Architect with the Malaysia Board of Architects. His research involves solar energy with the industrial sector and international collaboration with many organizations including Fraunhofer Solar Energy Research Institute, Germany. His expertise covers Building Integrated PV System (BIPV), Energy Efficiency in Buildings, Building Performance Simulation, Passive and Low Energy Architecture, Solar Assisted Air-Conditioning System, and Natural Ventilation.